

Development of Inductive Power Transfer System for Excavator under Large Load Fluctuation

-Consideration of relationship between load voltage and resonance parameter-

Jun-ichi Itoh¹, Kent Inoue^{2*} and Keisuke Kusaka²

¹ Department of Science of Technology Innovation Engineering

² Department of Electrical, Electronics and Information Engineering

Nagaoka University of Technology

Nagaoka, Niigata, Japan

*E-mail: k_inoue@stn.nagaokaut.ac.jp

Abstract— An inductive power transfer system for an excavator, which is operated under an air pressure environment, is designed and developed by considering the load voltage fluctuation. In the conventional excavator systems, the power is supplied via the contact wires, which may cause fire when a spark occurs because a working chamber environment is under high air pressure. In the proposed system, the series-parallel compensation is applied to cancel out the leakage inductance. By using the series-parallel compensation, the load voltage is ideally constant regardless of load fluctuation. However, the constant-voltage characteristic degrades due to winding resistance and an error of the resonance parameter. Thus, the resonance parameters have to be designed considering the error. In this paper, the design method of the resonance parameter is proposed with the voltage ratio maps considering the error of the parameter including the winding resistance. In the experiments with a developed 15-kW IPT system, the voltage fluctuation is smaller than 4.3%. Furthermore, the constant-voltage characteristic is maintained even when the output power of an induction motor changes from 5 kW to 15 kW and vice versa.

Keywords— Inductive power transfer, Excavator, Load fluctuation, Constant voltage characteristic

I. INTRODUCTION

A pneumatic caisson method is used in many structures: foundations of bridges and buildings, shafts for insertion of shield tunneling machines, tunnel and railways, e.g., the Chuo Shinkansen [1]. Figure 1 shows the schematic of the pneumatic caisson method. First, a reinforced concrete caisson is constructed on the ground. Second, an airtight working chamber is formed at the bottom of the caisson. Finally, the caisson is immersed at a predetermined depth and the pressurized air is supplied into the working chamber in order to prevent the underground water from coming into the chamber. Therefore, the working chamber environment is under high air pressure.

Figure 2 shows the schematic of the charging system. Fig. 2 (a) and (b) show the conventional charging system

and the proposed charging system, respectively. An excavator hangs onto the ceiling of the working chamber and moves along a traveling rail. Meanwhile, an electric hydraulic pump is used in order to move and operate the excavator. The power for an electric motor which drives hydraulic pump is supplied via an insulated trolley wire which is placed into the traveling rail. However, due to the movement of the excavator along the traveling rail, there is a threat of a spark which occurs at connection points. Even a small spark may cause a large-scale fire because the working chamber is under high air pressure environment. Therefore, in order to reduce the risk of the fire which is caused by the spark, the application of an inductive power transfer for the excavator has been proposed.

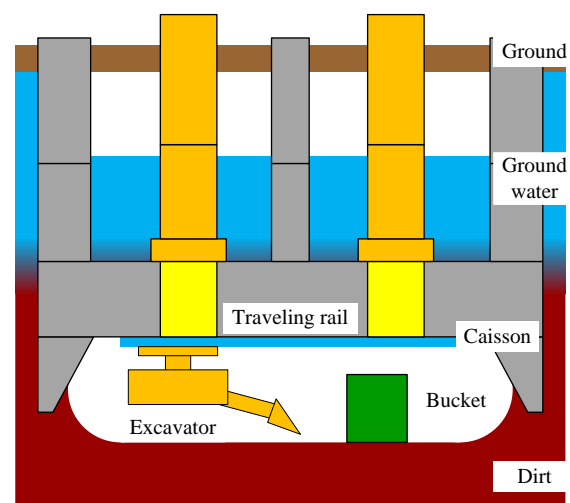


Fig. 1. Schematic of pneumatic caisson method which is immersed at predetermined depth and pressurized air is supplied into working chamber in order to prevent underground water from coming into chamber.

In the conventional method which is connected the capacitor in series to the primary side and the secondary side (SS compensation method), the secondary side features a constant-current characteristic when the primary side is driven at a constant voltage [2]–[4]. Therefore, the additional circuits, e.g., the buck converter and the boost converter, on the secondary side are required for the load voltage regulation. In addition, in the SS compensation method, the high-speed communication is needed between the primary side and the secondary side. On the other hand, the method which is connected the capacitor in series to the primary side and in parallel to the secondary side (SP compensation method) is regulated the load voltage without the additional circuits [5] [6]. Therefore, in the SP compensation method, the high-speed communication is unnecessary.

In this paper, the inductive power transfer system [7]–[14] for the excavator, which ensure the large load fluctuation, is developed. In the proposed system, the SP compensation is employed in order to cancel out the leakage inductance and a constant output voltage is ideally supplied even under the large load fluctuation without the

additional circuit. However, the constant-voltage characteristic degrades due to the winding resistance and the error of the resonance parameter.

The new contribution in this paper is providing an analysis how to develop the robust system against the voltage fluctuation. Analysis which is indicated this paper takes the relationship among the load fluctuation, the resonance parameter and the winding resistance takes into account in order to optimize parameters which is influenced the load voltage.

Based on the analysis on the voltage characteristic, a 15-kW inductive power transfer system is developed and tested. The constant load voltage characteristic is evaluated using a resistance and an induction motor load.

II. INDUCTIVE POWER TRANSFER SYSTEM FOR EXCAVATOR

A. System Configuration

Figure 3 shows the system configuration of the inductive power transfer system for the excavator. The proposed system consists of a converter with pulse-width

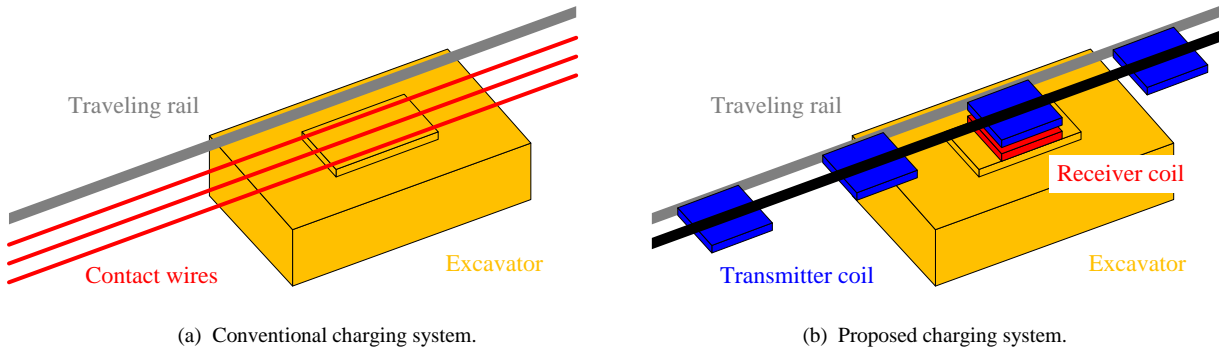


Fig. 2. Schematic of charging system which hangs onto ceiling of working chamber.

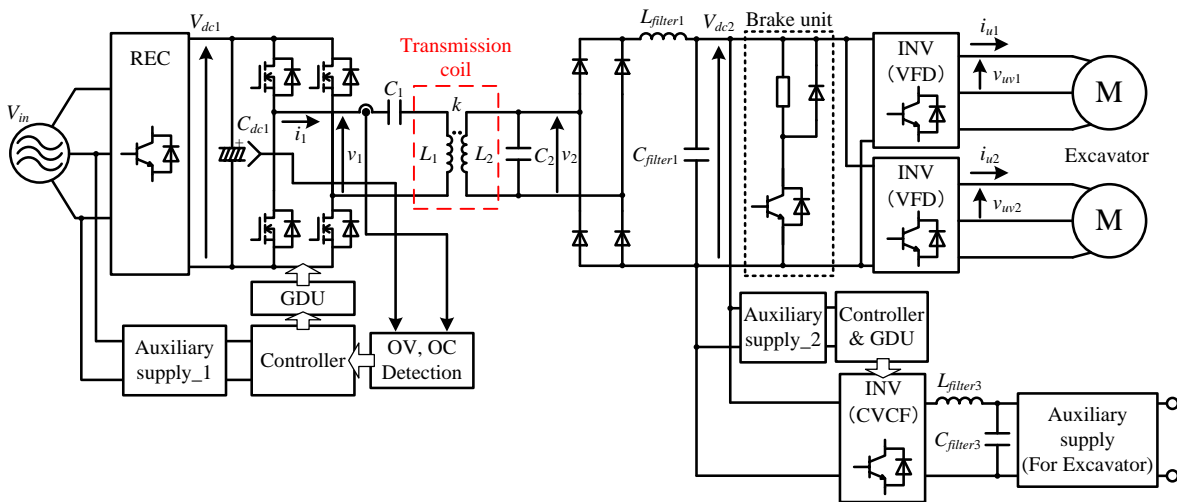


Fig. 3. Inductive power transfer system for excavator.

modulation (PWM) and a single-phase inverter in the primary side, a rectifier, a brake unit, a three-phase variable frequency drive (VFD) inverter and a single-phase constant voltage constant frequency (CVCF) inverter in the secondary side. The three-phase VFD inverters are used for adjustable speed driving an induction motors for an electric hydraulic pumps. The single-phase CVCF inverter is used as an auxiliary supply which is needed for an excavator control. The power is transferred from the primary side to the secondary side through the transmission coils. The SP compensation is employed in the system. Therefore, the secondary DC voltage is constant in the ideal conditions because the secondary side output features a constant-voltage characteristic regardless of a load fluctuation even if the primary side is driven at constant voltage. However, the winding resistance and an error of the resonance parameter practically degrade the constant-voltage characteristic.

B. Compensation Method of Reactive Power by Leakage Inductance of Transmission Coil

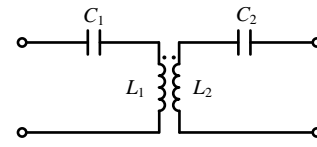
Figure 4 shows the typical compensation methods which is connected a resonance capacitor in series or parallel to the primary side coil and the secondary side coil in order to cancel out the reactive power [15]. Reactance components by leakage inductance are canceled out because of the resonance with the transmission coil. Consequently, the power factor seen from the primary side is.

Fig. 4 (a) shows the SS compensation method, which features a constant current characteristic at the secondary side when the primary side is driven at a constant voltage. Therefore, the SS compensation is unsuitable for the existing system because the additional circuit is needed in order to convert the constant current characteristic into the constant-voltage characteristic. In addition, the SS compensation is undesirable for the existing system because the high-speed communication is needed between the primary side and the secondary side. On the other hand, Fig. 4 (b) shows the SP compensation method, which features a constant voltage characteristic at the secondary side when the primary side is driven at a constant voltage. Therefore, the SP compensation is suitable to be applied to the proposed system because the inductive power transfer is possible to be applied into the existing excavator system without any modifications. However, the error of the resonance parameter needs to be considered.

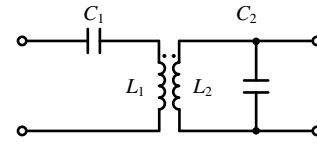
III. DESIGN OF TRANSMISSION COIL

A. Specifications

Figure 5 shows the transmission coil. An excavator system hangs onto the ceiling of the working chamber and moves along a traveling rail. Therefore, the upper side is the transmitter coil, the lower side is the receiver coil. In the proposed system, the solenoid coil is employed to obtain higher magnetic coupling in comparison with a circular coil. The cores are employed with PC40 manufactured by TDK. The size of the core is $W237 \times H210 \times D20$ mm. Meanwhile, the transmission distance is



(a) SS compensation.



(b) SP compensation.

Fig. 4. Typical compensation method which is connected capacitor in series or parallel in order to cancel out leakage inductance



Fig. 5. Transmission coils which is used core with PC40 manufactured by TDK. Upper side is transmitter coil, lower side is receiver coil. Coil size is $W237 \times H210 \times D20$ mm. Transmission distance is 50 mm.

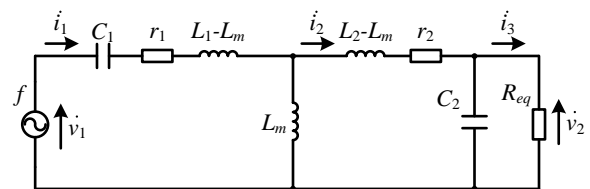


Fig. 6. Equivalent circuit of IPT system with SP compensation.

50 mm.

B. Parameters Design

Figure 6 shows the equivalent circuit for designing the IPT system. The circuit equations of the equivalent circuit which is shown Figure 6 are calculated as

$$V_1 = \left\{ r_1 + j\omega \left(L_1 - \frac{1}{\omega^2 C_1} \right) \right\} I_1 - j\omega L_m I_2 \dots\dots\dots (1),$$

$$0 = -j\omega L_m I_1 + \left\{ r_2 + j\omega \left(L_2 - \frac{1}{\omega^2 C_2} \right) \right\} I_2 + j \frac{1}{\omega C_2} I_3 \dots\dots\dots (2),$$

$$0 = j \frac{1}{\omega C_2} I_2 + \left(R_{eq} - j \frac{1}{\omega C_2} \right) I_3 \dots\dots\dots (3),$$

where V_1 is the primary voltage, R_{eq} is the equivalent load resistance, r_1 is the equivalent series resistance of the primary winding, r_2 is the equivalent series resistance of the secondary winding, L_1 is the primary inductance, L_2 is the secondary inductance, C_1 is the primary compensation capacitor, C_2 is the secondary compensation capacitor, L_m is the mutual inductance, and ω is the angular frequency of the power supply.

The currents I_1 , I_2 and I_3 are calculated by (4), (5) and (6) when an input voltage V_1 is applied into the primary side.

$$I_1 = \frac{V_1}{\Delta} \left[\left\{ r_2 + j(x_2 + x_0 - x_p) \right\} (R_{eq} - jx_p) + x_p^2 \right] \dots (4),$$

$$I_2 = \frac{V_1}{\Delta} jx_0 (R_{eq} - jx_p) \dots\dots\dots (5),$$

$$I_3 = \frac{V_1}{\Delta} x_0 x_p \dots\dots\dots (6),$$

$$\Delta = \begin{vmatrix} r_1 + j\omega \left(L_1 - \frac{1}{\omega^2 C_1} \right) & -j\omega L_m & 0 \\ -j\omega L_m & r_2 + j\omega \left(L_2 - \frac{1}{\omega^2 C_2} \right) & j \frac{1}{\omega C_2} \\ 0 & j \frac{1}{\omega C_2} & R_{eq} - j \frac{1}{\omega C_2} \end{vmatrix} \dots\dots\dots (7).$$

Note that the voltage V_1 is the fundamental component of the output voltage of the inverter.

The parameters of the transmission coil are designed with the equivalent circuit. The resistance R_{eq} indicates that equivalent load resistance considering the full-bridge rectifier. Then the equivalent load resistance is given by [16]

$$R_{eq} = \frac{\pi^2 V_{dc,2}^2}{8 P_2} \dots\dots\dots (8),$$

where $V_{dc,2}$ is the DC voltage on the secondary side and P_2 is the output power.

The inductances of the primary and the secondary coils are designed according to the following equations

$$L_2 = \frac{R_{eq}}{\omega} \frac{k}{\sqrt{1+k^2}} \dots\dots\dots (9),$$

$$L_1 = L_2 \left(\frac{8 V_{dc,1}}{\pi^2 k V_{dc,2}} \right)^2 \dots\dots\dots (10),$$

where $V_{dc,1}$ is the DC voltage on the primary side and k is the coupling coefficient.

The compensation capacitors are selected in order to cancel out the reactive power at the input frequency. Thus, the value of the compensation capacitors is calculated as

$$C_1 = \frac{1}{\omega^2 L_1 (1-k^2)} \dots\dots\dots (11),$$

$$C_2 = \frac{1}{\omega^2 L_2} \dots\dots\dots (12).$$

C. Influence of Parameter Error and Winding Resistance

Figure 7 shows the voltage ratio v_2/v_1 against the error of the resonance parameter including the winding resistance. Fig. 7 (a) and (b) show the v_2/v_1 ratio against the error of L_1 and C_1 and the error of L_2 and C_2 from 80% to 120%, respectively. Figure 7 represents the v_2/v_1 ratio which is calculated by (13) and (7).

$$\frac{v_2}{v_1} = \frac{R_{eq} \omega^2 L_m (L_1 - L_m)}{\Delta} \dots\dots\dots (13)$$

As a result of Fig. 7 (a), it is confirmed that v_2/v_1 ratio is high in a large area of the primary inductance L_1 and a small area of the primary capacitor C_1 . As a result of Fig. 7 (b), it is confirmed that v_2/v_1 ratio is high in a large area of the secondary inductance L_2 . Thus, in the resonance parameter of the secondary side, v_2/v_1 ratio depends on the secondary inductance L_2 . From the results, it is confirmed that the error of the resonance parameter affects v_2/v_1 ratio, i.e., the secondary DC voltage.

D. Coil size design

The size of the coil is decided based on the desired coupling coefficient and the transmission distance, which is obtained from the coupling coefficient maps [17]. The

core length is decided larger than the core depth because the coupling coefficient may be smaller than the design value.

IV. EXPERIMENTAL RESULTS

A. Experimental Conditions

Table I shows the experimental conditions. The rated power is 15 kW. The self-inductance of the primary side and the secondary side in Table I is measured value. In this experiment, a resistance or an induction motor is used as the load.

B. Resistance Load

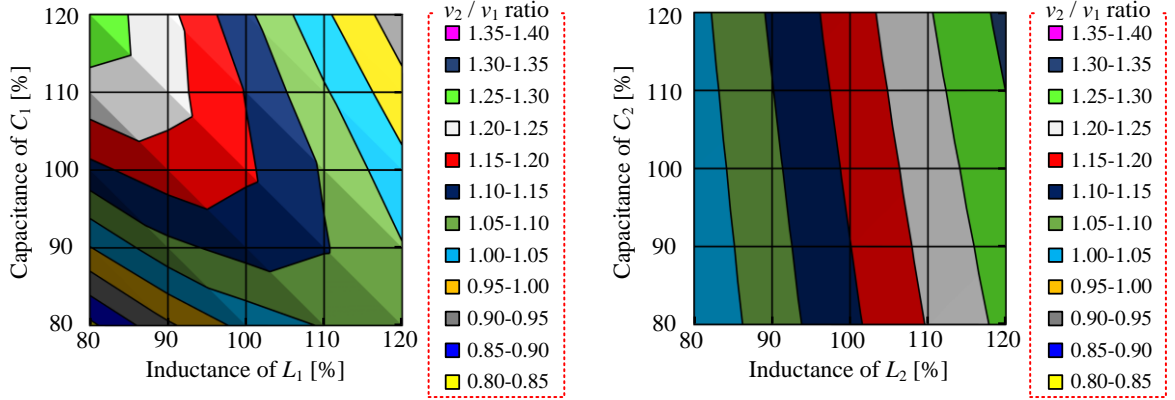
Figure 8 shows the operation waveforms with the resistance load. Fig. 8 (a) and (b) show the waveforms obtained at an output of 5 kW and 10 kW, respectively. In the figure, the secondary voltage is constant against the load power. Though the resonance condition is correct, the low-order harmonics affect the primary current in the light load. Therefore, the primary voltage and current

waveforms are misaligned from the resonance point.

Figure 9 shows the frequency characteristics of the voltage gain. Fig. 9 (a) and (b) show the input/output

TABLE I EXPERIMENTAL CONDITIONS.

	Symbol	Value
Switching frequency	f	20 kHz
Rated power	P	15 kW
Coupling coefficient	k	0.41
Primary inductance	L_1	393 μ H
Secondary inductance	L_2	113 μ H
Primary capacitance	C_1	198 nF
Secondary capacitance	C_2	582 nF
Primary winding resistance	r_1	107 m Ω
Secondary winding resistance	r_2	70 m Ω
MOSFETs		BSM120D12P2C005
Diodes		DH 2X61-18A



(a) Error of primary inductance L_1 and primary capacitor C_1 from 80% to 120%. (b) Error of secondary inductance L_2 and secondary capacitor C_2 from 80% to 120%.

Fig. 7. v_2 / v_1 ratio against error of resonance parameter including winding resistance. Graph legends shows v_2 / v_1 ratio.

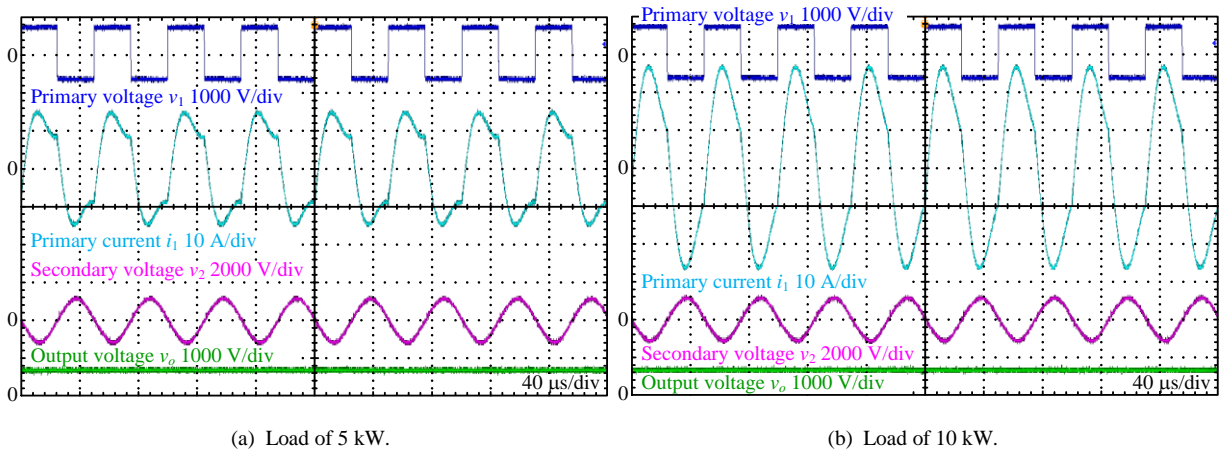


Fig. 8. Operation waveforms with resistance load.

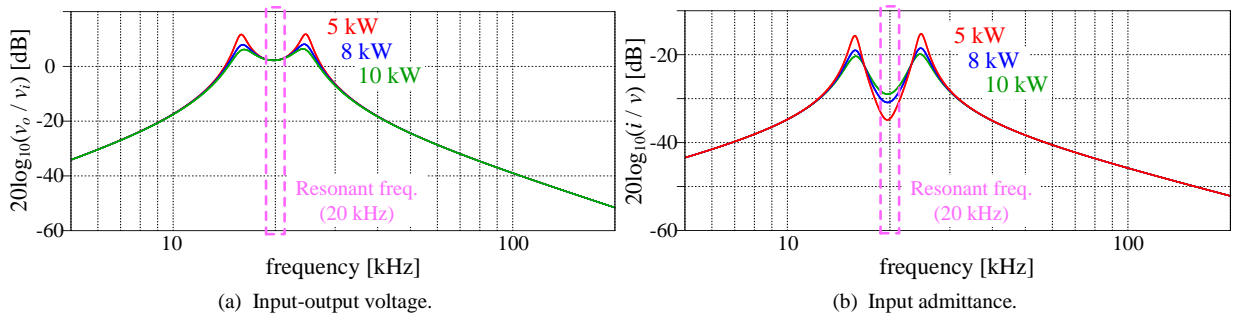


Fig. 9. Frequency characteristics of input-output voltage and input admittance gain

voltage ratio characteristic and the input admittance characteristic, respectively. The frequency characteristics in Fig. 9 are obtained in simulation in order to evaluate the effect of harmonics on the load. Around the fundamental frequency of the voltage gain frequency responses, the gain is same value regardless of the output power. On the other hand, it is concluded from the frequency characteristic of the input admittance; the gain around the fundamental frequency decreases at light load because low-order harmonics component of the input current is relatively large.

Figure 10 shows the frequency characteristics of the primary admittance. The gain of the fundamental component becomes smaller at light load, which has been expected from the frequency characteristics which is shown in Fig. 9 (b). Therefore, the distortion of the primary current at 5 kW is larger than the waveforms at 10 kW because low-order harmonics component of the primary current are relatively large at the light load.

Figure 11 shows the secondary/primary DC voltage ratio characteristic against the output power. The blue line in Fig. 11 represents the calculation value which is calculated without consideration of the resistance components in the rectifier. In the proposed system, the secondary/primary voltage ratio characteristic is expected to be constant because the SP compensation is employed in order to cancel out the leakage inductance. However, the secondary/primary DC voltage ratio decreases by 1.9% when the output power increases because the effect of voltage drop which is caused by the winding resistance is large at the high output power.

Figure 12 shows the secondary/primary voltage ratio characteristic against the output power. The blue line in Fig. 12 represents the calculation value by (13) and (7) using actual parameters considering the error from a nominal value. The green line in Fig. 12 represents calculation value which is calculated using (13) and (7) with design parameters (theoretical value). The experimental results agree with the calculation value of the prototype model with a small error (less than 0.5%). The error is caused by the difference between the nominal values and the actual values in the process of the resonance parameter design. Nevertheless, the secondary/primary voltage ratio characteristic is constant regardless of the output power. Therefore, it is confirmed that the decrease

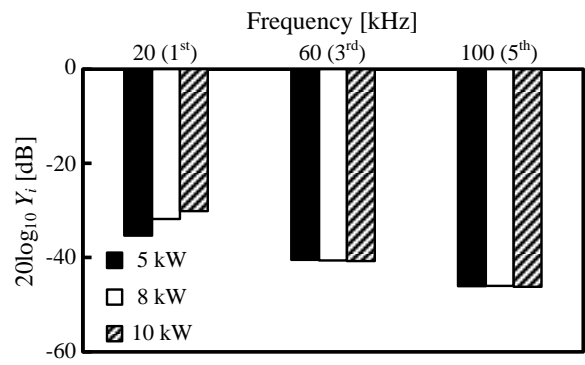


Fig. 10. Frequency characteristics of primary admittance. 1st: fundamental harmonic component (20 kHz), 3rd: triple harmonics component (60 kHz), 5th: fifth-order harmonics component (100 kHz)

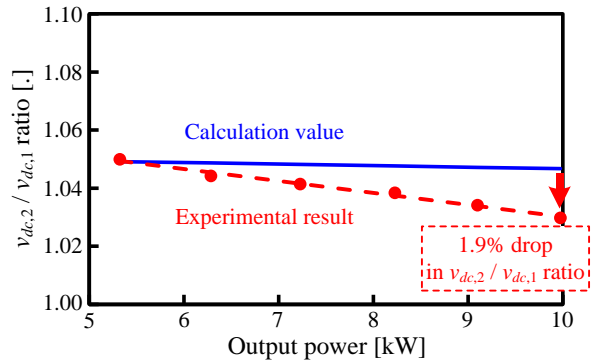


Fig. 11. Secondary/Primary DC voltage ratio. Red point is experimental results. Blue line is calculation value without consideration of resistance components in rectifier.

in the output/input voltage ratio at the high output power is mainly caused by the post-stage conversion, i.e., the rectifier.

Figure 13 shows the operation waveforms of the transient characteristic with the resistance load. Fig. 13 (a) and (b) show the step load response from 10 kW to 5 kW, and vice versa, respectively. The secondary DC voltage is maintained at constant even when the load step occurs. Consequently, it is confirmed that the secondary DC

voltage is constant regardless of the output power by using the SP compensation as a leakage inductance canceling method. In particular, the secondary DC voltage is constant even when a large load fluctuation occurs.

C. Induction Motor Load

Figure 14 shows the operation waveforms with the induction motor load which is connected to the pump. The output power is 15 kW. Fig. 14 (a) shows the primary voltage and current waveforms whereas Fig. 14 (b) shows the secondary DC voltage, output voltage and current waveforms. The primary current is confirmed that the waveform distortion is small because the fundamental components is relatively large, i.e. the influence of low-harmonics components is relatively small.

Figure 15 shows the operation waveforms of transient characteristic in the induction motor load. Fig. 15 (a) and (b) show the step response from 5 kW to 15 kW and vice versa, respectively. The secondary DC voltage is maintained at the constant value even when the load step occurs. Consequently, it is confirmed that the secondary

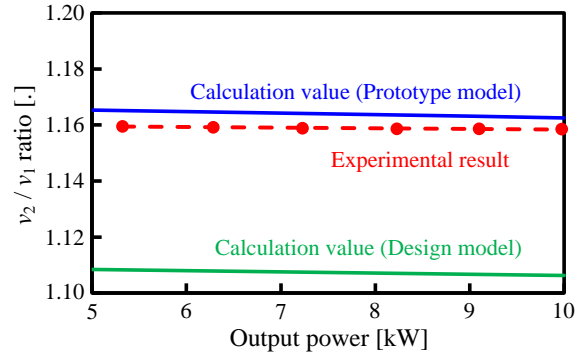
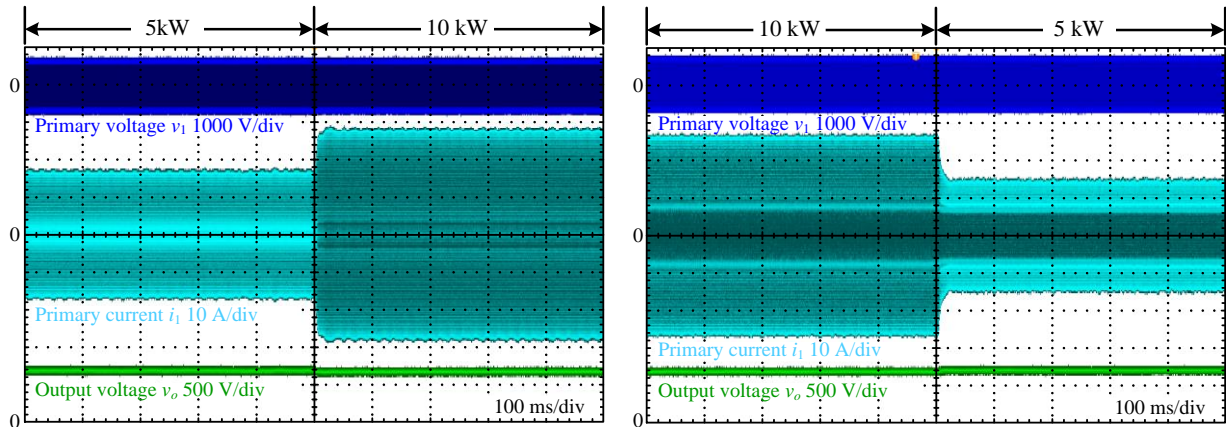


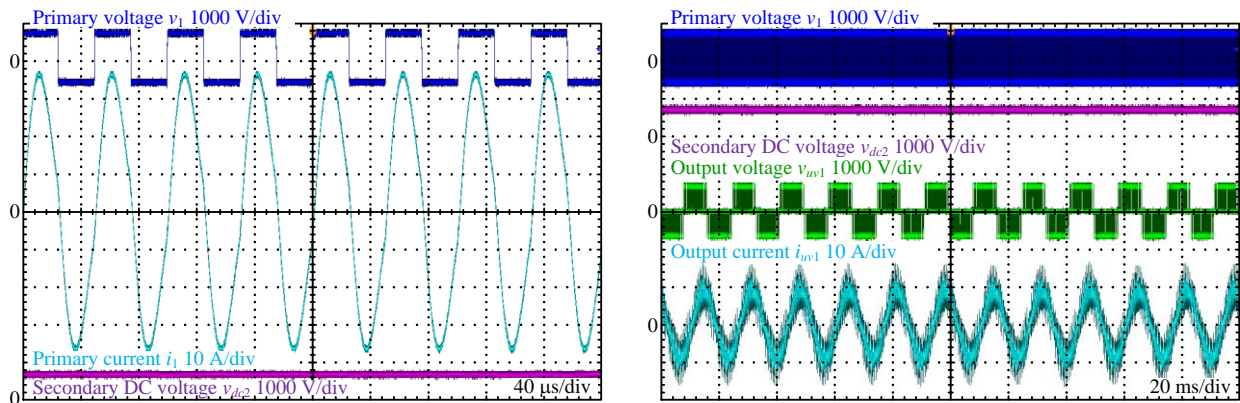
Fig. 12. Secondary/primary voltage ratio of transmission coil. Red point is experimental results. Blue line is calculation value by (13) and (7) using actual parameters considering error from nominal value. Green line is calculation value by (13) and (7) with design parameters.



(a) Step load response from 5 kW to 10kW.

(b) Step load response from 10 kW to 5 kW.

Fig. 13. Operation waveforms of transient characteristic with resistance load.



(a) Primary voltage and current waveform.

(b) Secondary DC voltage, output voltage and current waveform.

Fig. 14. Operation waveforms with induction motor load.

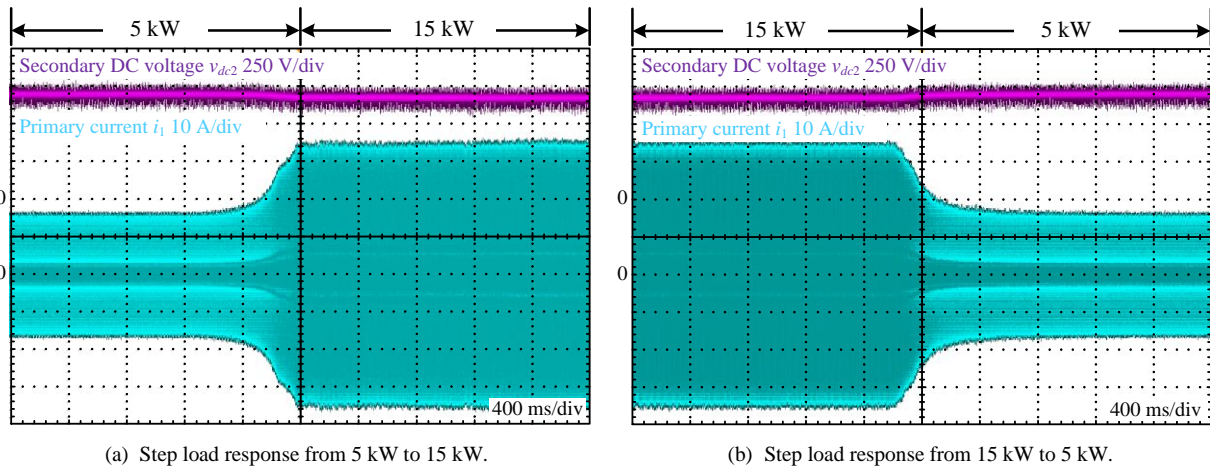


Fig. 15. Operation waveforms of transient characteristic with induction motor load.

DC voltage is constant regardless of the output power by using the SP compensation. In particular, the secondary DC voltage is constant even when a large load fluctuation occurs.

V. CONCLUSIONS

In this paper, the inductive power transfer system was applied in the existing excavator in order to reduce the fire risk which was caused by the spark of contact charging. In the proposed system, the load voltage against the load fluctuation should be stabilized without the additional circuit. In order to stabilize the load voltage against the load fluctuation, the SP compensation method was applied as the method in order to cancel out the leakage inductance. Moreover, the constant-voltage characteristic depending on the error of the resonance parameter and the winding resistance is theoretically analyzed in order to obtain the constant-voltage characteristic. In the experiments with an output power of 15 kW, the voltage fluctuation was smaller than 4.3%. The constant voltage is maintained even when the load step of the induction motor occurs, i.e. from 5 kW to 15 kW operation and vice versa. From the experimental results, the constant secondary DC voltage characteristic was confirmed, i.e. the constant output voltage.

REFERENCES

- [1] K. Kodaki, M. Nakano, S. Maeda: "Development of the automatic system for pneumatic caisson", ELSEVIER Automation in Construction, Vol. 6, No. 3, pp. 241-255, (1997).
- [2] K. Hata, T. Imura, Y. Hori: "Maximum Efficiency Control of Wireless Power Transfer via Magnetic Resonant Coupling Considering Dynamics of DC-DC Converter for Moving Electric vehicles", IEEE Applied Power Electronics Conference and Exposition, pp. 3301-3306, (2015)
- [3] M. Kato, T. Imura, Y. Hori: "Study on Maximize Efficiency by Secondary Side Control Using DC-DC Converter in Wireless Power Transfer via Magnetic Resonant Coupling", The International Electric Vehicle Symposium & Exhibition, (2013)
- [4] M. Sato, G. Guidi, T. Imura, H. Fujimoto: "Model for Loss Calculation of Wireless In-Wheel Motor Concept Based on Magnetic Resonant Coupling", IEEE Workshop on Control and Modeling for Power Electronics, No. 16267987, (2016)
- [5] T. Fujita, Y. Kaneko, S. Abe: "Contactless Power Transfer Systems using Series and Parallel Resonant Capacitors", IEEJ Trans. of Industry Applications, Vol. 127, No. 2, pp. 174-180, (2007).
- [6] R. Ota, N. Hoshi, J. Haruna: "Design of Compensation Capacitor in S/P Topology of Inductive Power Transfer System with Buck or Boost Converter on Secondary Side", IEEJ Journal of Industry Applications, Vol. 4, No. 4, pp. 476-485, (2015)
- [7] K. Kusaka, J. Itoh: "Development Trends of Inductive Power Transfer Systems Utilizing Electromagnetic Induction with Focus on Transmission Frequency and Transmission Power", IEEJ Transactions on Industry Applications, Vol. 137, No. 5, pp. 445-457, (2017).
- [8] S. Li, C. C. Mi: "Wireless Power Transfer for Electric Vehicle Applications", IEEE Journal, Vol. 3, No. 1, pp. 4-17, (2015)
- [9] D. Shimode, T. Murai, S. Fujiwara: "A Study of Structure of Inductive Power Transfer Coil for Railway Vehicles", IEEJ Journal of Industry Applications, Vol. 4, No. 5, pp. 550-558, (2015)
- [10] T. Mizuno, T. Ueda, S. Yachi, R. Ohtomo, Y. Goto: "Dependence of Efficiency on Wire Type and Number of Strands of Litz Wire for Wireless Power Transfer of Magnetic Resonant Coupling", IEEJ Journal of Industry Applications, Vol. 3, No. 1, pp. 35-40, (2014)
- [11] T. Koyama, K. Umetani, E. Hiraki: "Design Optimization Method for the Load Impedance to Maximize the Output Power in Dual Transmitting Resonator Wireless Power Transfer System", IEEJ Journal of Industry Applications, Vol. 7, No. 1, pp. 49-55, (2018)
- [12] S. Li, C. C. Mi: "Wireless Power Transfer for Electric Vehicle Applications", IEEE Journal, Vol. 3, No. 1, pp. 4-17, (2015)
- [13] A. Kurs, A. Karalis, R. Moffatt, J. D. Joannopoulos, P. Fisher, M. Soljacic: "Wireless Power Transfer via Strongly Coupled Magnetic Resonances", SCIENCE, Vol. 317, pp. 83-86, (2007)
- [14] K. Inoue, K. Kusaka, J. Itoh: "Reduction in Radiation Noise Level for Inductive Power Transfer Systems using Spread Spectrum Techniques", IEEE Transaction on Power Electronics, Vol. 33, No. 4, pp. 3076-3085, (2018)
- [15] T. Imura, Y. Hori: "Unified Theory of Electromagnetic Induction and Magnetic Resonant Coupling", IEEJ Trans. of Industry Applications, Vol. 135, No. 6, pp. 697-710, (2015).
- [16] R. Bosshard, J. W. Kolar, J. Muhlethaler, I. Stevanovic, B. Wunsch, F. Canales: "Modeling and η - α -Perato Optimization of Inductive Power Transfer Coils for Electric Vehicles", IEEE Transactions, Vol. 3, No. 1, pp. 50-64, (2015).
- [17] K. Inoue, K. Kusaka, D. Sato, J. Itoh: "Coupling Coefficient Maps for Wireless Power Transfer Using Solenoid Type Coil", IEICE Workshop on EE and WPT, No. WPT2016-34, pp. 85-90, (2016)